Microbial sulfate reduction plays an important role at the initial stage of subseafloor sulfide mineralization

Nozaki, Tatsuo ; Nagase, Toshiro ; Ushikubo, Takayuki ; Shimizu, Kenji ; Ishibashi, Jun-ichiro ; the D/V Chikyu Expedition 909 Scientists

(Citation)
Geology,49(2):222-227

(Issue Date)
2020-10-07

(Resource Type)
journal article

(Version)
Version of Record

GEOLOGY | THE GEOLOGICAL SOCIETY OF AMERICA®

https://doi.org/10.1130/G47943.1

Manuscript received 27 May 2020
Revised manuscript received 1 September 2020
Manuscript accepted 3 September 2020

Published online 7 October 2020

Microbial sulfate reduction plays an important role at the initial stage of subseafloor sulfide mineralization

Tatsuo Nozaki[1,2,3,4], Toshiro Nagase[5], Takayuki Ushikubo[6], Kenji Shimizu[6], Jun-ichiro Ishibashi[7], and the D/V Chikyu Expedition 909 Scientists

[1]Submarine Resources Research Center, Japan Agency for Marine-Earth Science and Technology (JAMSTEC), 2-15 Natsushima-cho, Yokosuka 237-0061, Japan
[2]Frontier Research Center for Energy and Resources, The University of Tokyo, 7-3-1 Hongo, Bunkyo-ku, Tokyo 113-8656, Japan
[3]Department of Planetology, Kobe University, 1-1 Rokkodai-cho, Nada-ku, Kobe 657-8501, Japan
[4]Ocean Resources Research Center for Next Generation, Chiba Institute of Technology, 2-17-1 Tsudanuma, Narashino 275-0016, Japan
[5]The Tohoku University Museum, Tohoku University, 6-3 Aoba, Aramaki, Aoba-ku, Sendai 980-8578, Japan
[6]Kochi Institute for Core Sample Research, JAMSTEC, Monobe-otsu 200, Nankoku 783-8502, Japan
[7]Department of Earth and Planetary Science, Kyushu University, 744 Motooka, Nishi-ku, Fukuoka 819-0395, Japan

ABSTRACT

Seafloor hydrothermal deposits form when hydrothermal fluid mixes with ambient seawater, and constituent sulfide minerals are usually interpreted to precipitate abiogenically. Recent research drilling at Izena Hole and Iheya North Knoll in the middle Okinawa Trough (East China Sea), combined with secondary ion mass spectrometry determinations of $\delta^{34}S$ in pyrite grains, provides compelling evidence that the initial stage of subseafloor sulfide mineralization is closely associated with microbial sulfate reduction. During the sulfide maturation process, pyrite textures progress from framboidal to colloform to euhedral. Pyrite $\delta^{34}S$ has highly negative values (as low as –38.9‰) in framboidal pyrite, which systematically increase toward positive values in colloform and euhedral pyrite. Sulfur isotope fractionation between seawater sulfate (+21.2‰) and framboidal pyrite (–38.9‰) is as great as –60‰, which can be attained only by microbial sulfate reduction in an open system. Because framboidal pyrite is commonly replaced by chalcopyrite, galena, and sphalerite, framboidal pyrite appears to function as the starting material (nucleus) of other sulfide minerals. We conclude that framboidal pyrite, containing microbially reduced sulfur, plays an important role at the initial stage of subseafloor sulfide mineralization.

INTRODUCTION

Modern seafloor massive sulfide (SMS) deposits are of interest as mineral resources due to their enrichment in Cu-Pb-Zn ± Au ± Ag. Volcanogenic massive sulfide (VMS) deposits are ancient and/or fossil examples of SMS deposits presently observed on land (Ohmoto, 1996; Piercey, 2011); both are formed by seafloor hydrothermal activity related to volcanism in mid-ocean-ridge and arc–back-arc settings (Tivey, 2007; Tornos et al., 2015). Sulfur isotope ($\delta^{34}S$) analyses of VMS deposits (Lode et al., 2017; Slack et al., 2019; Velasco-Acebes et al., 2019) have shown that an initial mineralization process characterized by the formation of framboidal pyrite (Piercey, 2015) is closely associated with microbial sulfate reduction. However, VMS deposits are subject to diagenesis and metamorphism during their emplacement on land, which can obscure the petrological (mineralogical) and geochemical records of their mineralization process. These early mineralization processes are best studied in SMS deposits, but systematic sampling from beneath the seafloor is possible only by costly deep-sea drilling campaigns.

Between 2010 and 2016, D/V *Chikyu* conducted drilling of sulfide deposits at Izena Hole and Iheya North Knoll, middle Okinawa Trough, East China Sea (Fig. 1A), as part of the International Ocean Drilling Program (IODP) Expedition 331 (Takai et al., 2011) and D/V *Chikyu* (JAMSTEC [Japan Agency for Marine-Earth Science and Technology] cruises CK14-04 (D/V *Chikyu* Expedition 907; Takai et al., 2015), CK16-01 (D/V *Chikyu* Expedition 908; Kumagai et al., 2017), and CK16-05 (D/V *Chikyu* Expedition 909; Nozaki et al., 2018). More than 800 m of obtained drill core provided evidence of the mineralization processes, especially the fate of sulfur, in the nascent stage of massive sulfide deposit formation. We also studied pyrite in sulfide chimneys at Iheya North Knoll that formed after the drilling operation at the same drill hole (IODP Hole C0016B) or at another drill hole (Hole C0016A) at the same site where the drill cores were obtained. Our textural observations and determinations of $\delta^{34}S$ in this material by *in situ* secondary ion mass spectrometry (SIMS) analysis demonstrate the importance and generality of microbial activity at the subseafloor sulfide formation.

GEOLOGICAL SETTING AND SAMPLES

The Okinawa Trough is a back-arc basin west of the Ryukyu arc in the East China Sea that extends >1200 km from the Japanese mainland to Taiwan (Fig. 1A). Owing to its slow extension rate of 3.7 ± 0.06 cm/yr (Kotake, 2000) and its geomorphological features (Arai et al., 2017), the Okinawa Trough is considered to be at the nascent stage of back-arc basin formation. The basin is divided into northern, middle, and southern segments by the Tokara Strait and Kerama Gap (Fig. 1A).

Our samples are drill cores from Izena Hole and cores and chimneys from Iheya North Knoll in the middle Okinawa Trough (Fig. 1A). Izena Hole (Fig. 1B) has two hydrothermal sites: the JADE site on the northeastern caldera slope (Halbach et al., 1989; Ishibashi et al., 2015) and the Hakurei site on the southern caldera floor (Ishibashi et al., 2015; Totsuka et al., 2019; Morozumi

CITATION: Nozaki, T., et al., 2021, Microbial sulfate reduction plays an important role at the initial stage of subseafloor sulfide mineralization: Geology, v. 49, p. 222–227, https://doi.org/10.1130/G47943.1

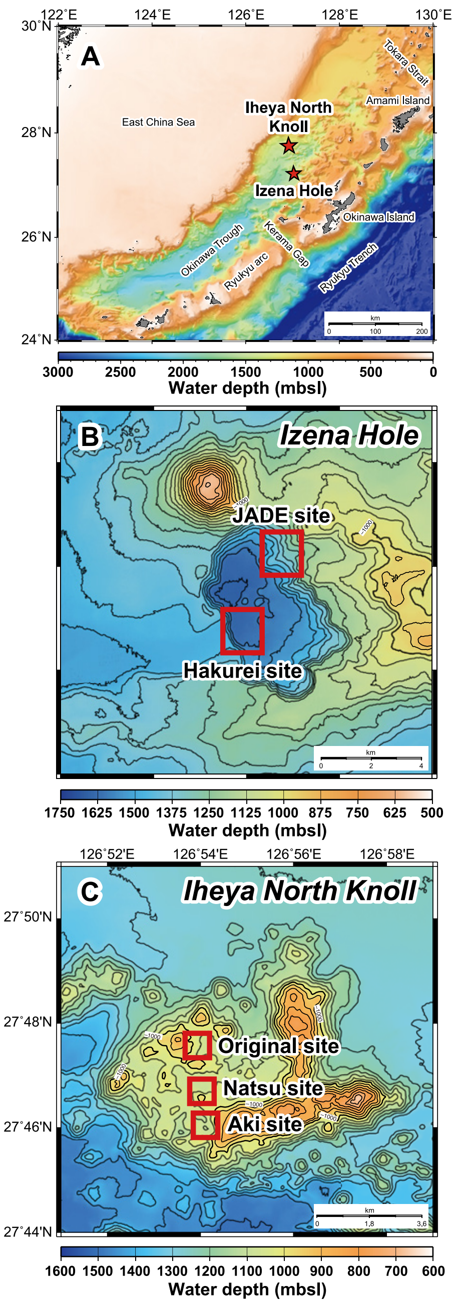

Figure 1. (A) Map of the Okinawa Trough, East China Sea. (B,C) Bathymetric maps of Izena Hole and Iheya North Knoll showing hydrothermal site locations. Modified from Nakamura et al. (2015). mbsl—meters below sea level.

et al., 2020). Iheya North Knoll (Fig. 1C) has three such sites: the Original, Natsu, and Aki sites (Nakamura et al., 2015). All five sites are active hydrothermal sites where the temperature of the hydrothermal fluid effluence exceeds 300 °C. The tectonics, geology, mineralization, and geochemistry of each hydrothermal field were reviewed by Ishibashi et al. (2015).

At Izena Hole, cores were obtained during D/V *Chikyu* Expedition 909 at the Hakurei site, from Hole C9027B on Northern mound and from Hole C9025A east of Northern mound and associated with a subseafloor sulfide body beneath the sediment (Figs. S1 and S2 and Tables S1–S3 in the Supplemental Material[1]) (Nozaki et al., 2018; Totsuka et al., 2019). At Iheya North Knoll, cores were drilled during IODP Expedition 331 at the Original site at Hole C0016B on the eastern flank of North Big Chimney mound (Figs. S1 and S3; Tables S1–S3) (Takai et al., 2011; Yeats et al., 2017). Young and infant chimneys at Holes C0016A and C0016B formed after the drilling operation at artificial hydrothermal vents (i.e., drill holes releasing hydrothermal fluid). Samples from these chimneys, which allow secular changes of mineral precipitation (chimney formation) and hydrothermal fluid geochemistry to be observed and *in situ* experiments to be conducted (Takai et al., 2011; Kawagucci et al., 2013), were collected 5, 11, and 18 months after the IODP Expedition 331 drilling during JAMSTEC research cruises KY11-02 Leg 3 (R/V *Kaiyo*), NT11-16 (R/V *Natsushima*), and NT12-06 (R/V *Natsushima*), respectively. Their petrographic and geochemical details are given by Nozaki et al. (2016).

Under the microscope, pyrite grains from the Hakurei site exhibit various textures (Fig. 2). In pumice fragments and in a sulfidic vein in the hanging wall above the subseafloor sulfide body, most pyrite has a framboidal texture and is accompanied by pyrrhotite pseudomorphs replaced by pyrite and marcasite (Fig. 2A). The framboidal pyrite is commonly overgrown by colloform and euhedral pyrite associated with sulfide maturation (Figs. 2B and 2C). This progression from framboidal to colloform and euhedral texture has also been reported in VMS deposits (Piercey, 2015; Velasco-Acebes et al., 2019). In drill cores from the Original site, paragenesis of framboidal and euhedral pyrite is observed in thin section (Fig. 2D), where framboidal pyrite is commonly replaced by chalcopyrite and galena, indicating that framboidal pyrite formed at an initial stage of sulfide mineralization (Halbach et al., 1993; Piercey, 2015). Chimneys from the Original site exhibit two distinct pyrite textures, colloform and/or spherical on the outer side and euhedral and/or acicular on the inner side (Figs. 2E and 2F).

ANALYTICAL METHODS

In situ $\delta^{34}S$ analysis was performed by SIMS (CAMECA IMS1280-HR) at the Kochi Institute for Core Sample Research, JAMSTEC (Nankoku, Japan). A primary $^{133}Cs^{+}$ ion beam with an intensity of 100 pA and total impact energy of 20 kV was focused to 2–3 µm in diameter at the sample surface. A gold coat ~30 nm thick was applied to the sample surface, and a normal-incidence electron gun was used for charge compensation. Secondary ions of two sulfur isotopes were accelerated at 10 kV and detected simultaneously by two Faraday cup (FC) detectors with 10^{11} Ω amplifiers (L1 for $^{32}S^{-}$ and optically axial FC2 for $^{34}S^{-}$). The entrance slit width was set at 61 µm. The exit slit widths were set at 500 and 243 µm for L1 and FC2, corresponding to a mass-resolving power of ~2200 and ~5000, respectively.

Each analysis consisted of 30 s for pre-sputtering, 50 s for centering of secondary ions in the field aperture, and 40 s for measurement (20 cycles with 2 s integration time). The typical intensity of $^{32}S^{-}$ was ~7×10^7 counts per second (cps) for pyrite analyses. Each group of nine to 21 sample analyses was bracketed by ten to 12 analyses of pyrite standard UWPy-1 (Ushikubo et al., 2014). Instrumental mass bias and analytical error were determined from average values and two standard deviations (SD) of the bracketing standard analyses. All data were normalized to the Vienna Canyon Diablo troilite (VCDT) standard. Typical uncertainty of $\delta^{34}S$ was ±0.4‰ (2SD). Detailed analytical and data reduction procedures were given by Ushikubo et al. (2014).

RESULTS AND DISCUSSION

The SIMS measurements yielded a total of 182 $\delta^{34}S$ values, representative examples of which are shown in Figure 3 (all measurement sites and data are shown in Figs. S4–S7 and listed in Tables S1–S3). Histograms of the $\delta^{34}S$ data, classified by pyrite texture, are shown in Figure 4. In the drill cores from the Hakurei site, $\delta^{34}S$ of framboidal pyrite ranged widely from –38.9‰ to –7.1‰ (average ± 1SD: –17.3‰ ± 10.2‰; $n = 42$) except in five analyses of highly recrystallized material. The colloform pyrite had a higher $\delta^{34}S$ range, from –13.6‰ to –3.0‰ (–7.4‰ ± 2.5‰; $n = 29$); similarly, $\delta^{34}S$ of euhedral pyrite ranged from –13.4‰ to –3.8‰ (–6.8‰ ± 2.7‰; $n = 19$), with one outlier. Recrystallized framboidal pyrite that consisted of several amalgamated grains (infilled framboidal pyrite; Wei et al., 2016) had $\delta^{34}S$ of ~–10‰ (Fig. 3B), similar to $\delta^{34}S$ of colloform and euhedral pyrites, whereas framboidal pyrite retaining its initial texture (normal framboidal pyrite; Wei et al., 2016) in the hanging-wall pumice fragments and sulfidic vein had the lowest $\delta^{34}S$ of ~–35‰ (Fig. 3A; Fig. S5). Similarly, in drill cores from the Original site, framboidal pyrite had lower $\delta^{34}S$ than euhedral pyrite (Figs. 3C and 4; Fig. S4). Unlike in the drill cores, however, pyrites in chimneys at this site had a narrow $\delta^{34}S$ range around 0‰, irrespective of their texture (Figs. 3D and 4; Fig. S7).

Given the $\delta^{34}S$ value of +21.2‰ in bottom-seawater sulfate at Iheya North Knoll (Aoyama et al., 2014), the sulfur isotope fractionation between seawater sulfate and framboidal pyrite was as great as –60‰, assuming the same $\delta^{34}S$ in seawater sulfate at Iheya North Knoll and Izena Hole. This fractionation factor is close

[1]Supplemental Material. Supplemental figures and tables. Please visit https://doi.org/10.1130/GEOL.S.12964949 to access the supplemental material, and contact editing@geosociety.org with any questions.

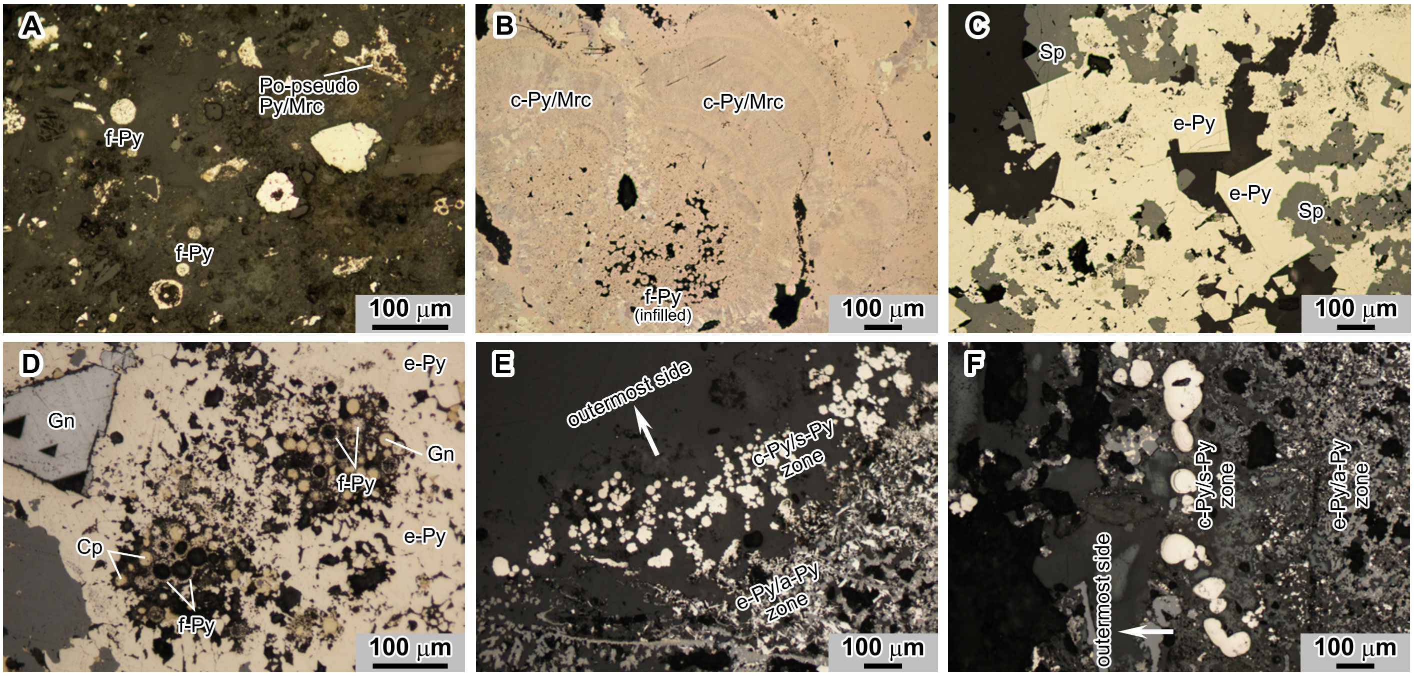

Figure 2. Reflected-light photomicrographs showing mineralogy and pyrite textures. (A) Framboidal pyrite and pyrrhotite pseudomorph replaced by pyrite and marcasite in sulfidic vein in a hanging wall above the subseafloor sulfide body from the Hakurei site (Okinawa Trough; sample 909-C9025A-3H-7-W, 58.0–60.0 cm [see Fig. S1; see footnote 1]). (B) Infilled framboidal pyrite and colloform pyrite and/or marcasite in subseafloor sulfide body from the Hakurei site (sample 909-C9025A-5H-3-W, 0.0–2.0 cm). (C) Euhedral pyrite associated with sphalerite at the Northern mound, Hakurei site (sample 909-C9027B-2X-CC-W, 15.0–17.0 cm). (D) Framboidal and euhedral pyrite from the eastern flank of North Big Chimney mound, Original site (Yeats et al., 2017) (sample 331-C0016B-1L-1-W, 17.0–19.0 cm). (E,F) Colloform and/or spherical pyrite on the outer side and euhedral and/or acicular pyrite on the inner side of chimneys at IODP Hole C0016A (sample HPD1355R03) (E) and Hole C0016B (sample HPD1247G01) (F), Original site (Nozaki et al., 2016). a—acicular; c—colloform; Cp—chalcopyrite; e—euhedral; f—framboidal; Gn—galena; Mrc—marcasite; Po—pyrrhotite; pseudo—pseudomorph; Py—pyrite; s—spherical; Sp—sphalerite.

to the largest values recorded in VMS deposits (–73‰ [Lode et al., 2017], –71‰ [Slack et al., 2019], –66‰ [Velasco-Acebes et al., 2019]). Three dominant sulfur sources for pyrite in SMS deposits have been considered: (1) magmatic sulfur in footwall rocks leached by hydrothermal fluid through water-rock interaction (δ^{34}S = 0‰ ± 3‰; Campbell and Larson, 1998; Shanks, 2001), (2) thermochemical (abiotic) sulfate reduction of anhydrite and/or gypsum and seawater sulfate by Fe^{2+}-bearing minerals or organic carbon, and (3) microbial sulfate reduction of seawater sulfate. A solely magmatic sulfur source to explain the highly negative δ^{34}S in framboidal pyrite can be ruled out at Izena Hole and Iheya North Knoll. δ^{34}S in abiotic H_2S depends on the degree of sulfate reduction, temperature, and δ^{34}S of S in anhydrite, gypsum, and seawater. The equilibrium fractionation factor between SO_4^{2-} and H_2S is estimated to be ~30‰ at 200 °C, ~25‰ at 250 °C, and ~20‰ at 350 °C, and abiotic sulfate reduction is kinetically inhibited below 200 °C (Ohmoto and Lasaga, 1982; Ohmoto, 1996). Because δ^{34}S in sulfate minerals (anhydrite and barite) at Izena Hole and Iheya North Knoll ranges from +16.3‰ to +25.5‰ (Zeng et al., 2000; Lüders et al., 2001; Ueno et al., 2003) and δ^{34}S of bottom-seawater sulfate is +21.2‰ (Aoyama et al., 2014), the δ^{34}S of –38.9‰ in framboidal pyrite could not have been produced abiotically. Thus, the strongly negative δ^{34}S in framboidal pyrite could have been produced only by microbial reduction of seawater sulfate. A repeated cycle of reduction of seawater sulfate to sulfide followed by sulfide oxidation (Canfield, 2001) in an open system with excess sulfate is the most plausible process to explain the extremely negative δ^{34}S in framboidal pyrite. An alternative process is single-step microbial sulfate reduction in an open system without sulfur disproportionation and reoxidation (Sim et al., 2011).

That framboidal pyrite is commonly replaced by other sulfide minerals such as chalcopyrite and galena (Fig. 2D) as well as sphalerite (Piercey, 2015) indicates that framboidal pyrite provides component material for other sulfide minerals. Our evidence suggests that framboidal pyrite incorporating S derived from microbial sulfate reduction serves as a nucleus for subsequent mineral growth at the initial stage of subseafloor sulfide mineralization. Colloform pyrite with δ^{34}S ~–7‰ is overgrown on framboidal pyrite as a result of overprinting by hydrothermal mineralization. We consider the S in colloform pyrite to be a mixture of magmatic S from rocks, as well as S from abiotic sulfate reduction of anhydrite and/or gypsum and seawater sulfate, with microbially reduced seawater sulfate. Euhedral pyrite in drill cores and chimneys has δ^{34}S of 0‰–3‰, explained by further overprinting by hydrothermal mineralization (and possibly additional S input through abiotic reduction). The interstitial water geochemistry of drill cores from the Hakurei site shows positive peaks of alkalinity and NH_4, H_2S, and CH_4 concentrations at 5–10 m above the subseafloor sulfide body, indicating that vigorous microbial sulfate reduction is taking place within the hanging-wall (pumiceous) sediment. Active subseafloor microbial sulfate reduction has also been confirmed by a multiple sulfur isotope study at the Original site (Aoyama et al., 2014) as well as at the Palinuro and Panarea hydrothermal fields in the Tyrrhenian Sea (Peters et al., 2011). The maximum fractionation in δ^{34}S between framboidal pyrite and seawater sulfate (–60‰) together with δ^{34}S evolution through the sulfide maturation process, observed in SMS and in VMS deposits on land (Lode et al., 2017; Slack et al., 2019; Velasco-Acebes et al., 2019), suggest that microbial activity is essential for SMS and VMS deposit formation and that microbial sulfate reduction plays an important role at the initial stage of mineralization beneath the seafloor sediments.

CONCLUSIONS

Microscopic evidence and δ^{34}S values in pyrite from Izena Hole and Iheya North Knoll indicate that pyrite progresses through framboidal, colloform, and euhedral textures accompanied by changes in δ^{34}S to higher values. Because

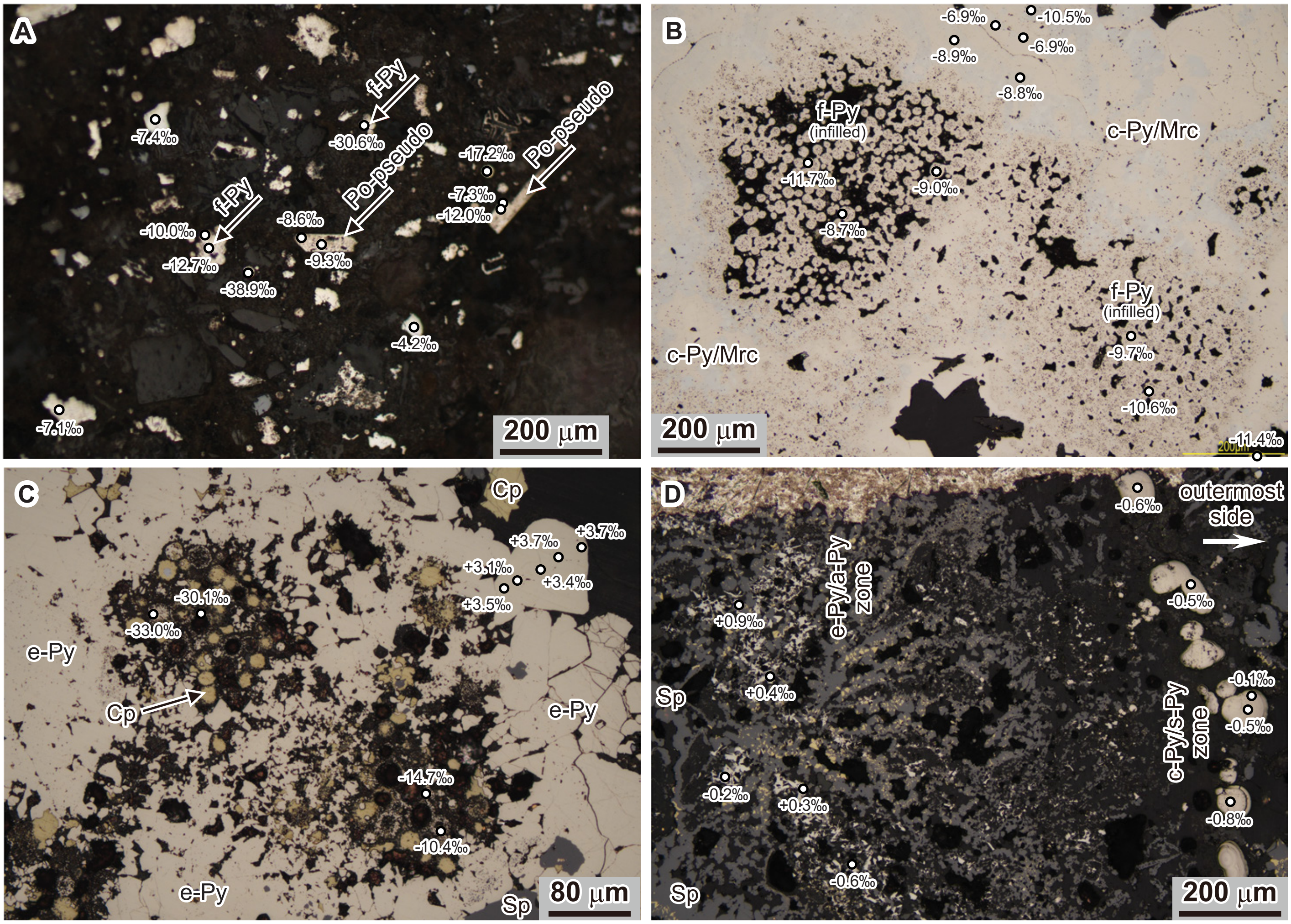

Figure 3. Reflected-light photomicrographs showing representative δ³⁴S values in pyrite determined by secondary ion mass spectrometry (SIMS). (A) Sample 909-C9025A-3H-7-W, 58.0–60.0 cm (see Fig. S1 [see footnote 1]). (B) Sample 909-C9025A-5H-3-W, 0.0–2.0 cm. (C) Sample 331-C0016B-1L-1-W, 17.0–19.0 cm. (D) Sample HPD1247G01. Abbreviations as in Figure 2.

δ^{34}S in framboidal pyrite as negative as –38.9‰ (or –60‰ with respect to seawater sulfate) could not have been produced by magmatic sulfur or abiotic sulfate reduction, the framboidal pyrite must be derived from seawater sulfate through microbial reduction in an open system. The ubiquity and abundance of framboidal pyrite with strongly negative δ^{34}S at the initial stage of sulfide mineralization in both SMS and VMS deposits can thus be explained by microbial sulfate reduction, and its widespread replacement by other sulfide minerals indicates that framboidal pyrite serves as a nucleus for subsequent mineral growth.

ACKNOWLEDGMENTS

We thank Yoshinori Ito of Tohoku University (Sendai, Japan) for producing the thin sections. We also thank the captains, crews, ROV operating teams, and technical staff of IODP Expedition 331 and JAMSTEC cruises KY11-02 Leg 3, NT11-16, NT12-06, and CK16-05 (D/V *Chikyu* Expedition 909) for their valuable collaboration. This study was supported by the Japan Society for the Promotion of Science through KAKENHI grants JP17K18814 and JP20H01999 to Ushikubo, and a grant-in-aid from the Japan Mining Promotional Foundation to Nozaki. This study was also supported by the Cross-Ministerial Strategic Innovation Project, the Council for Science, Technology and Innovation of the Japanese cabinet office, and by the IODP, which provided the samples. Constructive comments by three anonymous reviewers improved our manuscript.

REFERENCES CITED

Aoyama, S., Nishizawa, M., Takai, K., and Ueno, Y., 2014, Microbial sulfate reduction within the Iheya North subseafloor hydrothermal system constrained by quadruple sulfur isotopes: Earth and Planetary Science Letters, v. 398, p. 113–126, https://doi.org/10.1016/j.epsl.2014.04.039.

Arai, R., Kodaira, S., Kaiho, Y., Takahashi, T., Miura, S., and Kaneda, Y., 2017, Crustal structure of the southern Okinawa Trough: Symmetrical rifting, submarine volcano, and potential mantle accretion in the continental back-arc basin: Journal of Geophysical Research: Solid Earth, v. 122, p. 622–641, https://doi.org/10.1002/2016JB013448.

Campbell, A.R., and Larson, P.B., 1998, Introduction to stable isotope applications in hydrothermal systems: Reviews in Economic Geology, v. 10, p. 173–193, https://doi.org/10.5382/Rev.10.08.

Canfield, D.E., 2001, Biogeochemistry of sulfur isotopes: Reviews in Mineralogy and Geochemistry, v. 43, p. 607–636, https://doi.org/10.2138/gsrmg.43.1.607.

Halbach, P., et al., 1989, Probable modern analogue of Kuroko-type massive sulphide deposits in the Okinawa Trough back-arc basin: Nature, v. 338, p. 496–499, https://doi.org/10.1038/338496a0.

Halbach, P., Pracejus, B., and Marten, A., 1993, Geology and mineralogy of massive sulfide ores from the central Okinawa Trough, Japan: Economic Geology, v. 88, p. 2210–2225, https://doi.org/10.2113/gsecongeo.88.8.2210.

Ishibashi, J.-i., Ikegami, F., Tsuji, T., and Urabe, T., 2015, Hydrothermal activity in the Okinawa Trough back-arc basin: Geological background and hydrothermal mineralization, *in* Ishibashi, J.-i., et al., eds., Subseafloor Biosphere Linked to Hydrothermal Systems: New York, Springer, p. 337–359, https://doi.org/10.1007/978-4-431-54865-2_27.

Kawagucci, S., et al., 2013, Post-drilling changes in fluid discharge, mineral deposition patterns and fluid chemistry for the seafloor hydrothermal activity in the Iheya North hydrothermal field, Okinawa Trough: Geochemistry Geophysics Geosystems, v. 14, p. 4774–4790, https://doi.org/10.1002/2013GC004895.

Kotake, Y., 2000, Study on the tectonics of western Pacific region derived from GPS data analysis: Bulletin of the Earthquake Research Institute, University of Tokyo, v. 75, p. 229–334.

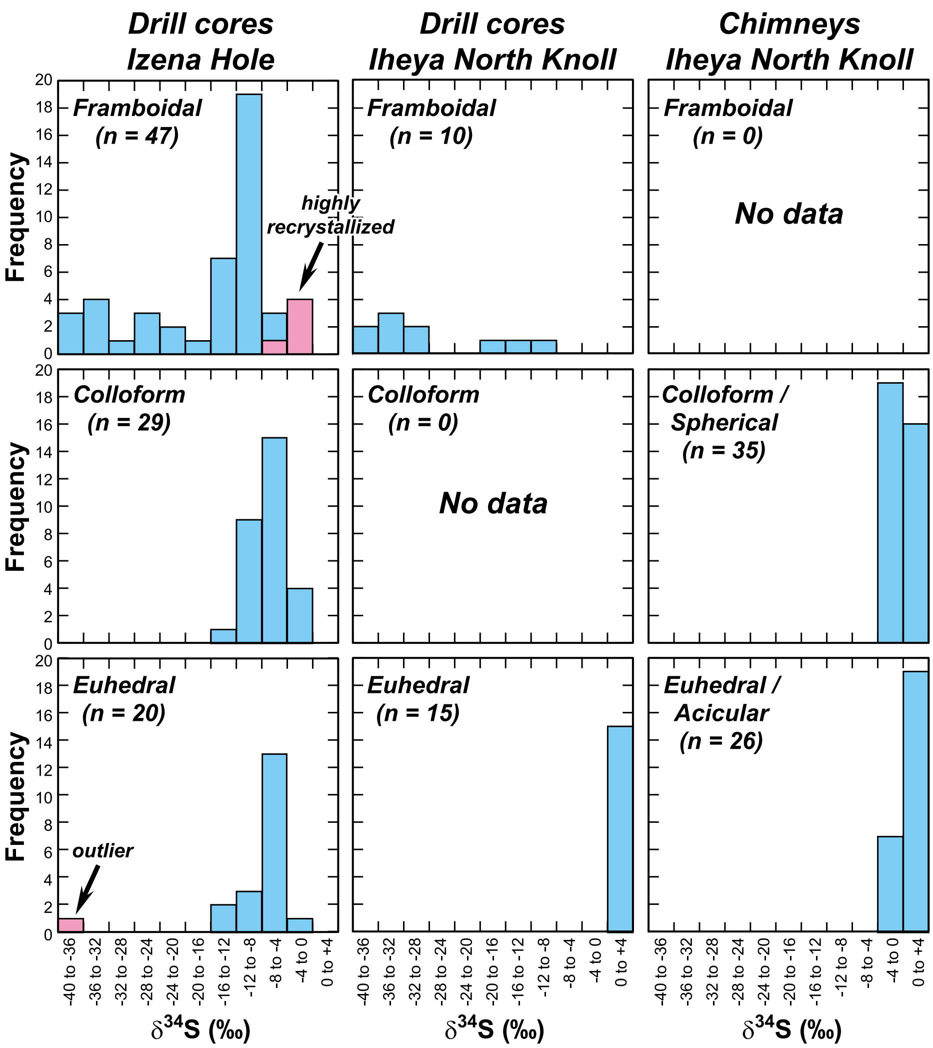

Figure 4. Histograms of δ³⁴S in pyrite textural categories. Pink bars in framboidal and euhedral pyrite of Izena Hole represent highly recrystallized framboidal pyrite values and outlier value, respectively.

Kumagai, H., Nozaki, T., Ishibashi, J.-i., Maeda, L., and CK16-01 on-board member, 2017, Cruise report SIP-HOT II "Explorer" (SIP–Hydrothermal deposit in Okinawa Trough) CK16-01 (Exp. 908): Yokosuka, Japan, JAMSTEC, 443 p.

Lode, S., Piercey, S.J., Layne, G.D., Piercey, G., and Cloutier, J., 2017, Multiple sulphur and lead sources recorded in hydrothermal exhalites associated with the Lemarchant volcanogenic massive sulphide deposit, central Newfoundland, Canada: Mineralium Deposita, v. 52, p. 105–128, https://doi.org/10.1007/s00126-016-0652-1.

Lüders, V., Pracejus, B., and Halbach, P., 2001, Fluid inclusion and sulfur isotope studies in probable modern analogue Kuroko-type ores from the JADE hydrothermal field (Central Okinawa Trough, Japan): Chemical Geology, v. 173, p. 45–58, https://doi.org/10.1016/S0009-2541(00)00267-9.

Morozumi, H., Ishikawa, N., Chiba, M., Watanabe, K., Ogata, T., Takahashi, R., and Ishibashi, J.-i., 2020, Characteristics of ore deposits for marine mineral resources investigated by JOGMEC since 2014: Shigen-Chishitsu, v. 70, p. 53–65.

Nakamura, K., Kawagucci, S., Kitada, K., Kumagai, H., Takai, K., and Okino, K., 2015, Water column imaging with multibeam echo-sounding in the mid-Okinawa Trough: Implications for distribution of deep-sea hydrothermal vent sites and the cause of acoustic water column anomaly: Geochemical Journal, v. 49, p. 579–596, https://doi.org/10.2343/geochemj.2.0387.

Nozaki, T., et al., 2016, Rapid growth of mineral deposits at artificial seafloor hydrothermal vents: Scientific Reports, v. 6, 22163, https://doi.org/10.1038/srep22163.

Nozaki, T., Takaya, Y., Nagase, T., Yamasaki, T., Ishibashi, J.-I., Kumagai, H., Maeda, L., and CK16-05 Cruise Members, 2018, Subseafloor mineralization beneath hemipelagic sediments at the Izena Hole, middle Okinawa Trough, observed through the CK16-05 Cruise (Exp. 909): Abstract V33A-01 presented at 2018 Fall Meeting, American Geophysical Union, Washington, D.C., 10–14 December.

Ohmoto, H., 1996, Formation of volcanogenic massive sulfide deposits: The Kuroko perspective: Ore Geology Reviews, v. 10, p. 135–177, https://doi.org/10.1016/0169-1368(95)00021-6.

Ohmoto, H., and Lasaga, A.C., 1982, Kinetics of reactions between aqueous sulfates and sulfides in hydrothermal systems: Geochimica et Cosmochimica Acta, v. 46, p. 1727–1745, https://doi.org/10.1016/0016-7037(82)90113-2.

Peters, M., Strauss, H., Petersen, S., Kummer, N.-A., and Thomazo, C., 2011, Hydrothermalism in the Tyrrhenian Sea: Inorganic and microbial sulfur cycling as revealed by geochemical and multiple sulfur isotope data: Chemical Geology, v. 280, p. 217–231, https://doi.org/10.1016/j.chemgeo.2010.11.011.

Piercey, S.J., 2011, The setting, style, and role of magmatism in the formation of volcanogenic massive sulfide deposits: Mineralium Deposita, v. 46, p. 449–471, https://doi.org/10.1007/s00126-011-0341-z.

Piercey, S.J., 2015, A semipermeable interface model for the genesis of subseafloor replacement-type volcanogenic massive sulfide (VMS) deposits: Economic Geology, v. 110, p. 1655–1660, https://doi.org/10.2113/econgeo.110.7.1655.

Shanks, W.C., III, 2001, Stable isotopes in seafloor hydrothermal systems: Vent fluids, hydrothermal deposits, hydrothermal alteration, and microbial processes: Reviews in Mineralogy and Geochemistry, v. 43, p. 469–525, https://doi.org/10.2138/gsrmg.43.1.469.

Sim, M.S., Bosak, T., and Ono, S., 2011, Large sulfur isotope fractionation does not require disproportionation: Science, v. 333, p. 74–77, https://doi.org/10.1126/science.1205103.

Slack, J.F., Shanks, W.C., III, Ridley, W.I., Dusel-Bacon, C., DesOrmeau, J.W., Ramezani, J., and Fayek, M., 2019, Extreme sulfur isotope fractionation in the Late Devonian Dry Creek volcanogenic massive sulfide deposit, central Alaska: Chemical Geology, v. 513, p. 226–238, https://doi.org/10.1016/j.chemgeo.2019.03.007.

Takai, K., Mottl, M.J., Nielsen, S.H., and the Expedition 331 Scientists, 2011, Proceedings of the Integrated Ocean Drilling Program, Volume 331: Tokyo, Integrated Ocean Drilling Program Management International, Inc., https://doi.org/10.2204/iodp.proc.331.2011.

Takai, K., Kumagai, H., Kubo, Y., and CK14-04 onboard member, 2015, Cruise report SIP-HOT I "Pathfinder" (SIP–Hydrothermal deposit in Okinawa Trough) CK14-04 (Exp. 907): Yokosuka, Japan, JAMSTEC, 116 p.

Tivey, M.K., 2007, Generation of seafloor hydrothermal vent fluids and associated mineral deposits: Oceanography (Washington, D.C.), v. 20, p. 50–65, https://doi.org/10.5670/oceanog.2007.80.

Tornos, F., Peter, J.M., Allen, R., and Conde, C., 2015, Controls on the siting and style of volcanogenic massive sulphide deposits: Ore Geology Reviews, v. 68, p. 142–163, https://doi.org/10.1016/j.oregeorev.2015.01.003.

Totsuka, S., Shimada, K., Nozaki, T., Kimura, J.-I., Chang, Q., and Ishibashi, J.-i., 2019, Pb isotope compositions of galena in hydrothermal deposits obtained by drillings from active hydrothermal fields in the middle Okinawa Trough determined by LA-MC-ICP-MS: Chemical Geology, v. 514, p. 90–104, https://doi.org/10.1016/j.chemgeo.2019.03.024.

Ueno, H., Hamasaki, H., Murakawa, Y., Kitazono, S., and Takeda, T., 2003, Ore and gangue minerals of sulfide chimneys from the North Knoll, Iheya Ridge, Okinawa Trough, Japan: JAMSTEC Journal of Deep Sea Research, v. 22, p. 49–62.

Ushikubo, T., Williford, K.H., Farquhar, J., Johnston, D.T., Van Kranendonk, M.J., and Valley, J.W., 2014, Development of in situ sulfur four-isotope analysis with multiple Faraday cup detectors by SIMS and application to pyrite grains in a Paleoproterozoic glaciogenic sandstone: Chemical Geology, v. 383, p. 86–99, https://doi.org/10.1016/j.chemgeo.2014.06.006.

Velasco-Acebes, J., Tornos, F., Kidane, A.T., Wiedenbeck, M., Velasco, F., and Delgado, A., 2019, Isotope geochemistry tracks the maturation of submarine massive sulfide mounds (Iberian

Pyrite Belt): Mineralium Deposita, v. 54, p. 913–934, https://doi.org/10.1007/s00126-018-0853-x.
Wei, H.Y., Wei, X.M., Qiu, Z., Song, H.Y., and Shi, G., 2016, Redox conditions across the G–L boundary in South China: Evidence from pyrite morphology and sulfur isotopic compositions: Chemical Geology, v. 440, p. 1–14, https://doi.org/10.1016/j.chemgeo.2016.07.009.
Yeats, C.J., Hollis, S.P., Halfpenny, A., Corona, J.-C., LaFlamme, C., Southam, G., Fiorentini, M., Herrington, R.J., and Spratt, J., 2017, Actively forming Kuroko-type volcanic-hosted massive sulfide (VHMS) mineralization at Iheya North, Okinawa Trough, Japan: Ore Geology Reviews, v. 84, p. 20–41, https://doi.org/10.1016/j.oregeorev.2016.12.014.
Zeng, Z.G., Jiang, F.Q., Zhai, S.K., Qin, Y.S., and Hou, Z.Q., 2000, Sulfur isotopic composition of seafloor hydrothermal sediment from the Jade hydrothermal field in the central Okinawa Trough and its geological significance: Acta Oceanologica Sinica, v. 22, p. 74–82.

Printed in USA